BMC Methods

METHODOLOGY

Open Access

Mosquito Tissue Ultrastructure-Expansion Microscopy (MoTissU-ExM) enables ultrastructural and anatomical analysis of malaria parasites and their mosquito

Benjamin Liffner[1], Thiago Luiz Alves e Silva[2], Joel Vega-Rodriguez[2*] and Sabrina Absalon[1*]

Abstract

Background Study of malaria parasite cell biology is challenged by their small size, which can make visualisation of individual organelles difficult or impossible using conventional light microscopy. In recent years, the field has attempted to overcome this challenge through the application of ultrastructure expansion microscopy (U-ExM), which physically expands a biological sample approximately 4.5-fold. To date, U-ExM has mostly been used to visualise blood-stage parasites and used exclusively on parasites in vitro.

Methods Here we develop Mosquito Tissue U-ExM (MoTissU-ExM), a method for preparing dissected mosquito salivary glands and midguts by U-ExM. MoTissU-ExM preserves both host and parasite ultrastructure, enabling visualisation of oocysts and sporozoites in situ. We also provide a point-by-point protocol for how to perform MoTissU-ExM.

Results We validate that MoTissU-ExM samples expand as expected, provide a direct comparison of the same dissected tissues before and after MoTissU-ExM, and highlight some of the key host and parasite structures that can be visualised following MoTissU-ExM.

Discussion We discuss potential use cases for MoTissU-ExM for study of malaria parasite biology, and more broadly. We detail drawbacks or challenges MoTissU-ExM and imaging these expanded tissues, along with information troubleshooting this technique. Finally, we discuss how MoTissU-ExM could be applied and adapted in future to increase its utility.

Keywords Plasmodium, Expansion microscopy, Tissue microscopy, Vector biology, Imaging, Mosquito, Malaria

Introduction

Cell biology is fundamentally underpinned by our ability to visualise cells and use this information to infer biological structure and function. Light microscopy, the visualisation of cells based on the light they emit or absorb, is one of the most widely used tools in cell biology. Historically, the ability of light microscopy to resolve biological structures had been bounded by diffraction limit of light [1]. Over the last few decades, however, many methods that overcome this limit, collectively called "super-resolution" microscopy, have been developed. Typically, super-resolution microscopy techniques involve the use of

*Correspondence:
Joel Vega-Rodriguez
Joel.Vega-Rodriguez@nih.gov
Sabrina Absalon
Sabsalon@iu.edu
[1] Department of Pharmacology & Toxicology, Indiana University School of Medicine, Indianapolis, IN 46202, USA
[2] Molecular Parasitology & Entomology Unit, Laboratory of Malaria & Vector Research, NIH-NIAID, Rockville, MD 20852, USA

some form of specialised instrumentation or analysis to improve resolution and therefore the ability to visualise biological structures [2]. In 2015, however, a conceptually different method called expansion microscopy (ExM) was developed [3]. Rather than use specialised instrumentation, ExM is a sample preparation method that physically expands a biological sample; resulting in a dramatic increase in the ability to resolve biological structures without the need for specialised equipment.

Since the initial development of ExM, many adaptations to and variations of ExM have been published. Notably, ultrastructure expansion microscopy (U-ExM) [4] has been widely applied to the study of single-celled organisms [5–12]. U-ExM involves the tethering of a biological sample to a hydrogel using formaldehyde and acrylamide, before denaturation, expansion and staining. Importantly for its use in single-celled organisms, U-ExM results in near-native preservation of cellular ultrastructure and 4 to 4.5-fold isotropic expansion [4].

U-ExM has been widely adopted in the study of the cell biology of apicomplexan parasites [13]. Apicomplexa are a phylum of largely parasitic single-celled organisms that include significant causes ofdisease in humans and livestock, such as malaria, toxoplasmosis and cryptosporidiosis. To date, U-ExM has been used to study the cell biology of *Plasmodium* [6, 14, 15], *Toxoplasma* [16, 17], *Cryptosporidium* [7, 18], and *Neospora* [19]. To date, U-ExM has only been applied to parasites cultured in vitro and prepared as either isolated parasites or infected-cell monolayers. Being able to observe the anatomical context these parasites exist in, however, is key to understanding both parasite biology and host-parasite interactions. Here, we develop a method we call Mosquito Tissue U-ExM (MoTissU-ExM), a protocol tailored to visualise the ultrastructure of malaria parasites (*Plasmodium*) and their mosquito hosts in situ. We validate that this method fully expands the mosquito tissues and we test a range of commonly used fluorescent dyes and stains. Finally, we provide a point-by-point protocol for dissecting, preparing, and imaging expanded mosquito tissues. While developed for malaria parasites, the application of MoTissU-ExM could extend across various fields of entomological and parasitological research.

Results

U-ExM has been applied to different stages of the malaria parasite lifecycle but not to either mosquito midgut oocysts or salivary gland sporozoites. Whole tissues have previously been visualised using U-ExM [20], including zebrafish and mouse embryos, and *Drosophila* wings, but this involved modifications to the U-ExM protocol that more than doubled sample processing time. We reasoned that dissected mosquito midguts and salivary glands are enclosed epithelial monolayers and, therefore, would not require the extensive processing required for thicker tissues.

Development of mosquito tissue U-ExM (MoTissU-ExM)

We then developed a pipeline for the dissection, fixation, gelation, expansion, and imaging of both infected mosquito midguts and salivary glands (Fig. 1) (see point-by-point protocol). Briefly, dissected mosquito tissues were fixed in 4% v/v paraformaldehyde before in-solution anchoring in formaldehyde/acrylamide. Anchored tissues were concentrated and transferred to 12 mm Ø poly-D-lysine-coated coverslips (approx. 5 tissues per coverslip). Excess anchoring solution was removed, tissues were evenly spaced apart, and underwent gelation. Following gelation, gels were placed in denaturation buffer to separate the gel and coverslip. Once gels had separated from the coverslip, each infected tissue (still visible in the gel) was cut out of the gel for individual denaturation, expansion, staining, and imaging.

While fundamentally MoTissU-ExM builds on already established U-ExM protocols, we made some minor modifications specifically for this application. These modifications include a streamlined processing pipeline from fixation to anchoring where both steps occur in solution prior to transfer to a coverslip. This change was to minimise moving tissues around to preserve their structural integrity. Additionally, in solution fixation and anchoring were favoured because the dissected mosquito tissues adhered poorly to poly-D-lysine coated coverslips. Further modifications were made to concentrate and separate multiple tissues on the same coverslip, followed by cutting out and processing of each tissue individually. Following denaturation, MoTissU-ExM is the same as other U-ExM protocols with the caveat that the gel pieces are much smaller and therefore require smaller antibody and wash solution volumes. Finally, we developed some guidelines for imaging of MoTissU-ExM samples based on the challenges we experienced in the development of this method.

Dissected mosquito tissues expand fully

When a sample is appropriately denatured in the U-ExM protocol, the diameter of the expanded gel divided by the diameter of the unexpanded gel can be used as a guide for the expansion factor of the biological sample [6]. For this method, mosquito tissues were cut individually from the gel, hence the expansion factor could not be estimated in this way. To determine the expansion factor of mosquito tissues prepared by U-ExM, we measured the average diameter of nuclei in both unexpanded and U-ExM midguts (Fig. 2) and salivary glands (Fig. 3). Additionally, we measured the

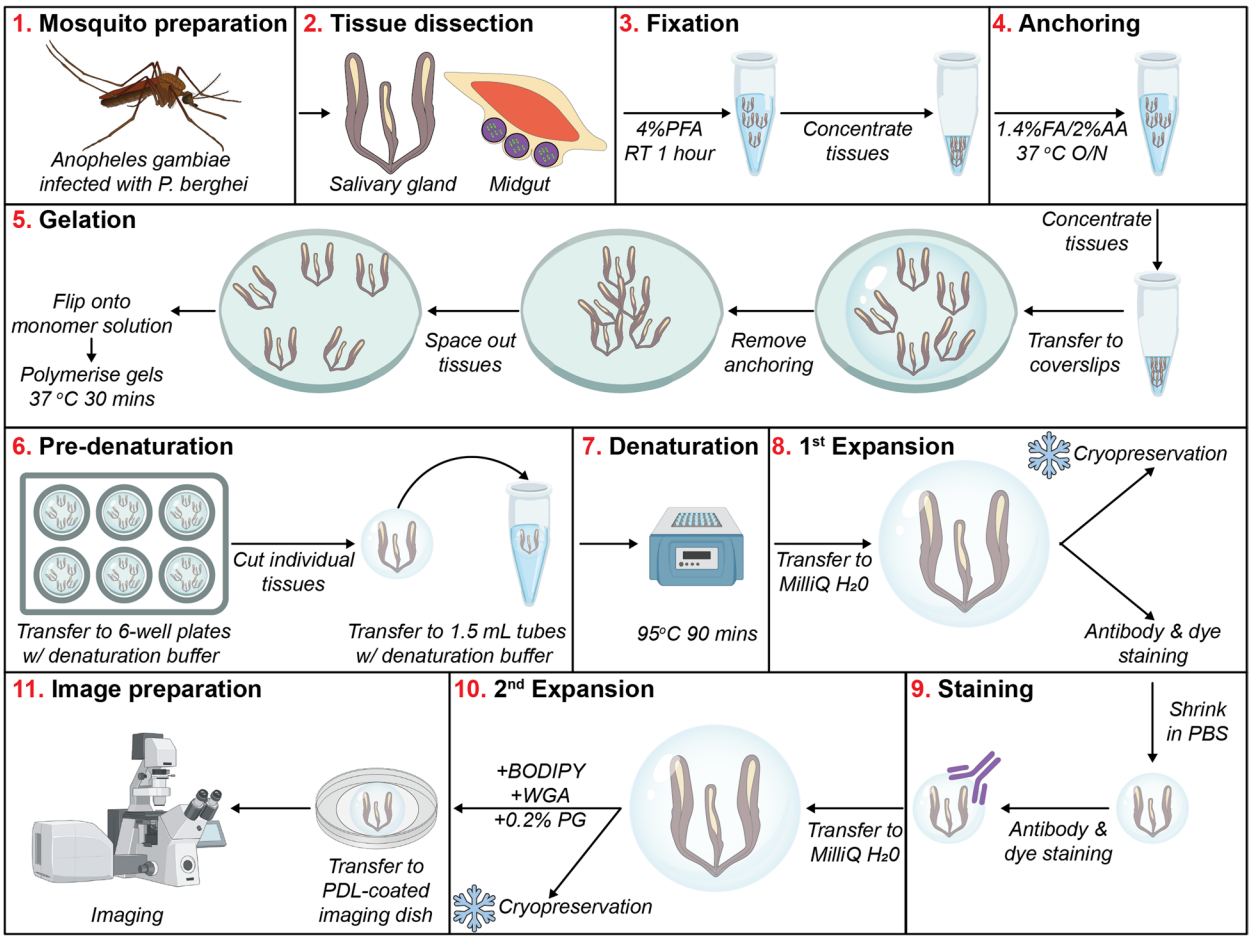

Fig. 1 Workflow for preparing Mosquito Tissues using U-ExM (MoTissU-ExM). Workflow diagram for the dissection, preparation, and expansion of mosquito tissues. Note that the workflow alternates between being read left to right (steps **1.** – **4.** and **6.** – **8.**) and right to left (steps **5.** And **9.** to **11.**) between rows. A detailed step-by-step text version of this process can be found in the methods section. Steps **3.** – **11.** depict salivary glands, but the process is the same for midguts. Longitudinal opening of midguts is not depicted in this workflow. PFA: paraformaldehyde, RT: room temperature: FA: formaldehyde, AA: acrylamide, O/N: overnight, DI H2O: deionised water, PBS: phosphate buffered saline, WGA: wheat germ agglutinin, PG: propyl gallate. Snowflakes indicate stages where gels can be cryopreserved at -20 °C

same nucleus in a salivary gland (Fig. 2a) or a midgut (Fig. 3a), both before and after expansion. In unexpanded midguts (Fig. 2b), the average midgut epithelial cell nucleus diameter was 7.252 µm (± SD 1.57 µm, 200 nuclei, 4 midguts), while the average nucleus diameter in U-ExM midguts was 31.62 µm (± SD 5.79 µm, 200 nuclei, 4 midguts). In unexpanded salivary glands (Fig. 3b), the average salivary gland epithelial cell nucleus diameter was 10.17 µm (± SD 1.66 µm, 179 nuclei, 4 salivary glands), while the average nucleus diameter in U-ExM salivary glands was 42.63 µm (± SD 8.35 µm, 176 nuclei, 5 salivary glands). This estimates an average linear expansion factor of 4.19-fold for salivary glands and 4.36-fold for midguts across multiple experiments. These expansion factors are consistent with those previously published using U-ExM [4, 6, 14, 21] and suggest that mosquito tissues prepared using U-ExM are fully expanded.

U-ExM of mosquito tissues preserves both parasite and host ultrastructure

Highly chitinous tissues from arthropods can be resistant to isotropic expansion [22], introducing sample distortions. Given that nuclei expanded as expected, it was unlikely that chitin was limiting expansion in mosquito salivary glands or midguts, but we wanted to confirm that both the host tissue and the parasites were being preserved at both the anatomical and ultrastructural levels.

To first confirm that sporozoite ultrastructure was preserved following U-ExM, we prepared and imaged purified salivary gland sporozoites using a conventional U-ExM protocol. In previous U-ExM studies, parasite

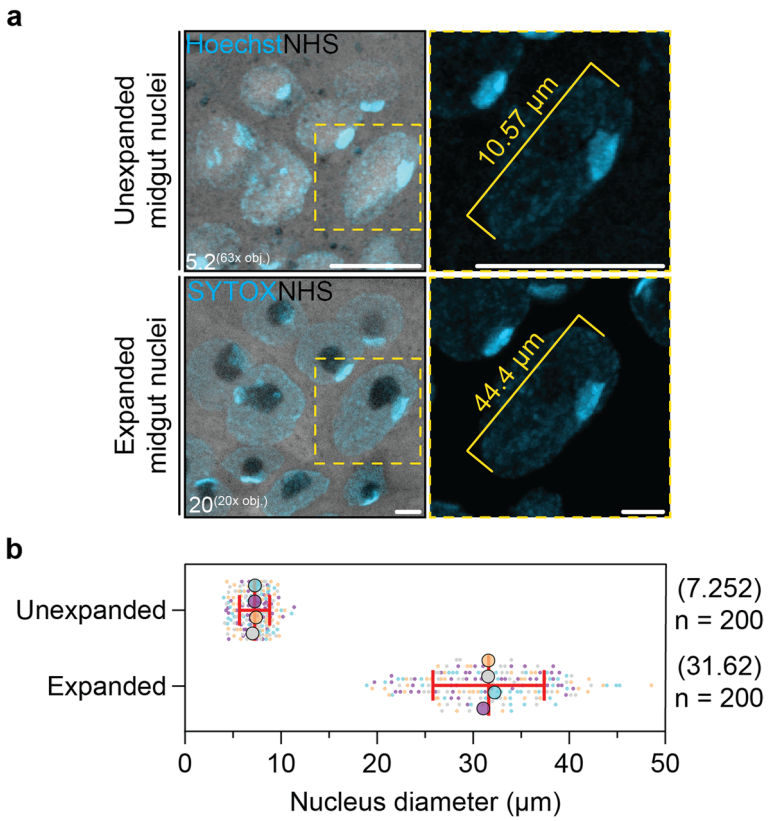

Fig. 2 Measuring expansion factor of MoTissU-ExM midguts. **a** To determine the expansion factor of midguts prepared by U-ExM, unexpanded midguts were stained with Hoechst (cyan, DNA) and NHS ester Alexa Fluor 405 (greyscale, protein density), and imaged by Airyscan 2 microscopy. U-ExM midguts were stained with SYTOX (cyan, DNA) and NHS ester. The same nucleus, before and after U-ExM is depicted. Number in the bottom corner of each image indicates z-projection depth in µm. obj. = objective lens (see methods section for objective lens details). Scale bar = 10 µm. **b** Maximum midgut nucleus diameter was measured in both unexpanded and U-ExM midguts, giving an average estimated expansion factor of 4.36-fold. Approximately 50 nuclei from 4 unexpanded and U-ExM midguts were measured. Small datapoints represent individual nuclei measurements, while large datapoints represent midgut means. Error bars = SD

ultrastructure has been observed using dyes that are not protein specific, such as NHS Ester or BODIPY ceramide [6, 14, 23, 24]. In these cases, parasite ultrastructure has shown a striking resemblance to previously published transmission electron microscopy (TEM) studies. Leveraging these observations, we imaged purified sporozoites stained with NHS ester and BODIPY ceramide (Fig. 4). By comparing against previously published TEM images of sporozoites [25–29], we confirmed that in U-ExM sporozoites we could visualise a number of subcellular structures including: the nucleus, the rhoptries, the Golgi, the apical polar rings (APR), and the basal complex (Fig. 4). Preservation of all these subcellular features in a manner indistinguishable from TEM confirm the sporozoite ultrastructure is preserved following U-ExM. In addition to clearly distinguishable features in sporozoites prepared by U-ExM, we observed many protein-dense granular structures (Fig. 4). Based on protein density staining alone it is currently unclear if these represent micronemes, dense granules, other secretory/trafficking vesicles, or a combination of the three.

In U-ExM midguts, both large anatomical features like muscle fibres and fine anatomical features like microvilli were preserved (Fig. 5) in a manner similar to previous electron microscopy studies [30, 31]. Additionally, *P. berghei* oocysts were well preserved with the oocyst capsule along with developing sporozoites and their DNA (Fig. 5). For a more detailed comparison, we imaged the same midgut, same oocyst, and same forming sporozoites both before (Fig. 6a) and after (Fig. 6b) expansion. The entire midgut, along with the relative position of all host cells and oocysts within that midgut appeared highly preserved with no significant aberrations observed at either the anatomical or ultrastructural levels.

Similarly to midguts, both salivary gland morphology and ultrastructure were preserved following U-ExM. In expanded salivary glands, lateral and medial lobes were easily distinguished from each other, with a clear

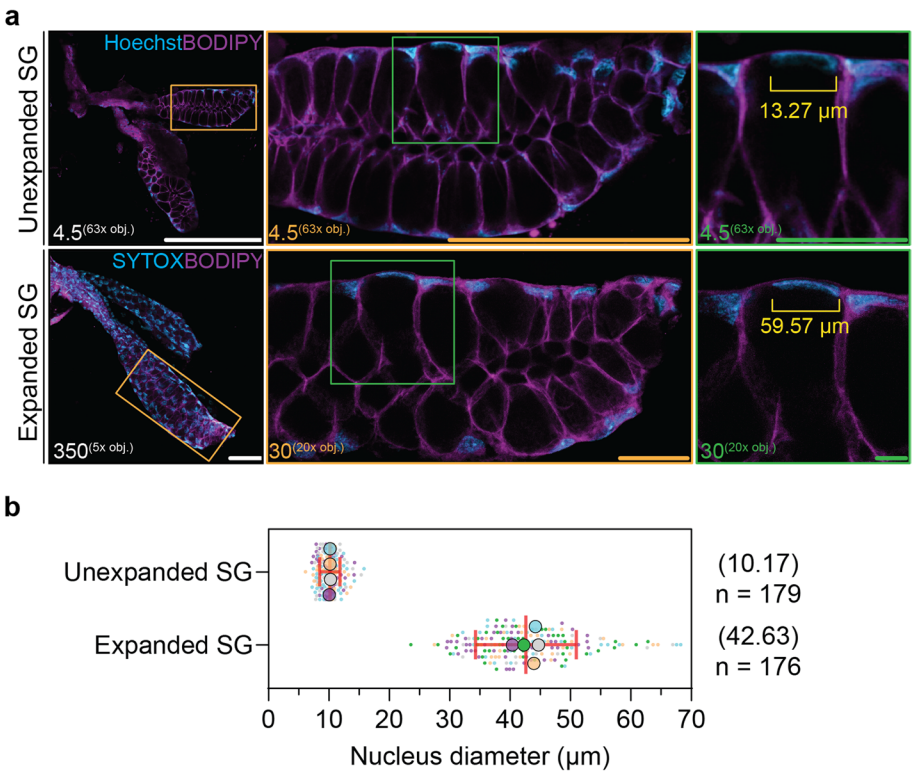

Fig. 3 Measuring expansion factor of MoTissU-ExM salivary glands. **a** To determine the expansion factor of salivary glands prepared by U-ExM, unexpanded midguts were stained with Hoechst (cyan, DNA) and BODIPY-FL-Ceramide (magenta, lipids), and imaged by Airyscan microscopy. U-ExM salivary glands were stained with SYTOX (cyan, DNA) and BODIPY. The same salivary gland, before and after U-ExM, is depicted (note that salivary gland orientation changed during U-ExM preparation) with a zoom of the same lateral lobe (orange) and same nucleus (green). Number in the bottom corner of each image indicates z-projection depth in µm. obj. = objective lens. Scale bars: white = 200 µm, orange = 50 µm, green = 20 µm. **b** Maximum salivary gland nucleus diameter was measured in both unexpanded and U-ExM salivary glands, giving an average estimated expansion factor of 4.19-fold. 179 nuclei from 4 unexpanded salivary glands, and 176 nuclei from 5 U-ExM salivary glands were measured. Small datapoints represent individual nuclei measurements, while large datapoints represent salivary gland means. Error bars = SD

distinction between the distal and proximal regions of those lobes (Fig. 7). Further, throughout the whole salivary gland, the secretory cavity could be easily distinguished from the cytoplasm of the epithelial cells just by using stains for protein density, wheat germ agglutinin (WGA), or lipids (BODIPY) (Fig. 7). For sporozoites in expanded salivary glands, their relative position (epithelial cell cytoplasm or secretory cavity) could easily be visualised (Fig. 8). We learned that reimaging the same salivary gland before and after expansion did not provide a clear anatomical comparison as it did for midguts. Although we successfully imaged the same salivary gland before and after expansion (Fig. 3a), this method presented challenges. Each lobe of the salivary gland had independent mobility from its original imaging to expansions. Therefore, it was challenging to correlate the anatomical structures between the initial and expanded states of the salivary glands (Fig. 6).

Addressing challenges of sample depth

For the implementation of this protocol, the most significant technical hurdle we faced was imaging expanded tissues, especially salivary glands, due to the depth of the expanded sample combined with the shallow limit of the working distance of an oil immersion objective. This means that typically, only a very small portion of the expanded mosquito tissue is accessible using a standard high-resolution imaging setup. A typical high-resolution confocal microscope setup would include a high numerical aperture (NA) oil-immersion objective (such as the 63x, 1.4 NA objective used in this study), with a working distance of < 200 µm. Following expansion, the distance from the start of the gel to the basal side of the tissue is always significantly greater than 200 µm (typically 500 – 1000 µm). This effect is amplified in salivary glands, which are frequently suspended within the gel rather than lying flat on one surface.

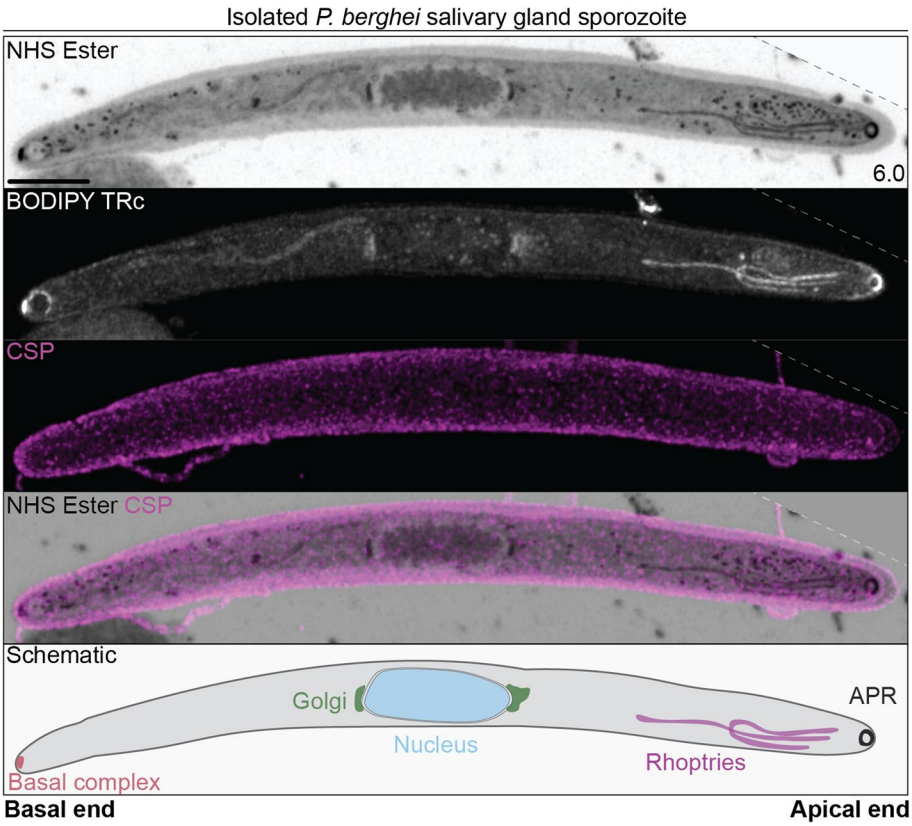

Fig. 4 U-ExM of purified sporozoites. To determine if sporozoite ultrastructure was preserved following U-ExM, isolated salivary gland sporozoites were prepared by U-ExM and stained with NHS Ester (greyscale, protein density) and BODIPY-Tr-Ceramide (white, lipids) and anti-circumsporozoite antibodies (magenta, sporozoite surface), and imaged by Airyscan microscopy. Number in the bottom corner of each image indicates z-projection depth in µm. Scale bars = 5 µm. APR = Apical polar rings. This image was rotated for the purpose of presentation, a dashed line marks the edge of the acquired image

To mitigate this limitation for mosquito midguts, we first tried longitudinally 'opening' the midgut following dissection. We reasoned that opened midguts would lay flat within the gel, with both sides imageable on a high-resolution imaging setup. Longitudinally opened midguts were compatible with U-ExM (Fig. 9) and, in some instances dramatically increased the area of the expanded midgut accessible using a 63 × oil-immersion objective lens. In many instances, however, the edges of the longitudinally opened midgut curled and made even less of the tissue accessible using a 63 × oil-immersion objective lens.

While we could frequently observe *P. berghei* oocysts within an expanded midgut, using a 63 × oil-immersion objective lens, we could never image the entirety of the oocyst depth as it would exceed the objective working distance (Fig. 10a). To overcome this, we utilised a 40 × water-immersion (1.2 NA) objective lens with a ~ 500 µm working distance. Using this 40 × objective, we were able to measure the depth of an oocyst (Fig. 10b) that we could not measure using the 63 × oil-immersion objective. Additionally, despite the 40 × water-immersion objective having a lower NA, the image was markedly brighter and clearer than using the 1.4 NA 63 × objective (Fig. 10). This is to be expected as the NA of an objective assumes refractive index matching between immersion and the sample. As the gel is mostly water, this means the effective NA of the 63 × oil-immersion is < 1.4, and in this instance likely marginally lower than the effective NA of the 40 × water-immersion objective lens.

Discussion

Broader applications of MoTissU-ExM

Here, we developed the first protocol for in situ visualisation of mosquito tissues and the malaria parasites within them using ultrastructure expansion microscopy (MoTissU-ExM). For the oocysts imaged in this study we focussed primarily on relatively developed oocysts that had begun sporogony, as it is easier to visualise parasite ultrastructure at this stage. Despite this, the MoTissU-ExM is equally compatible with the

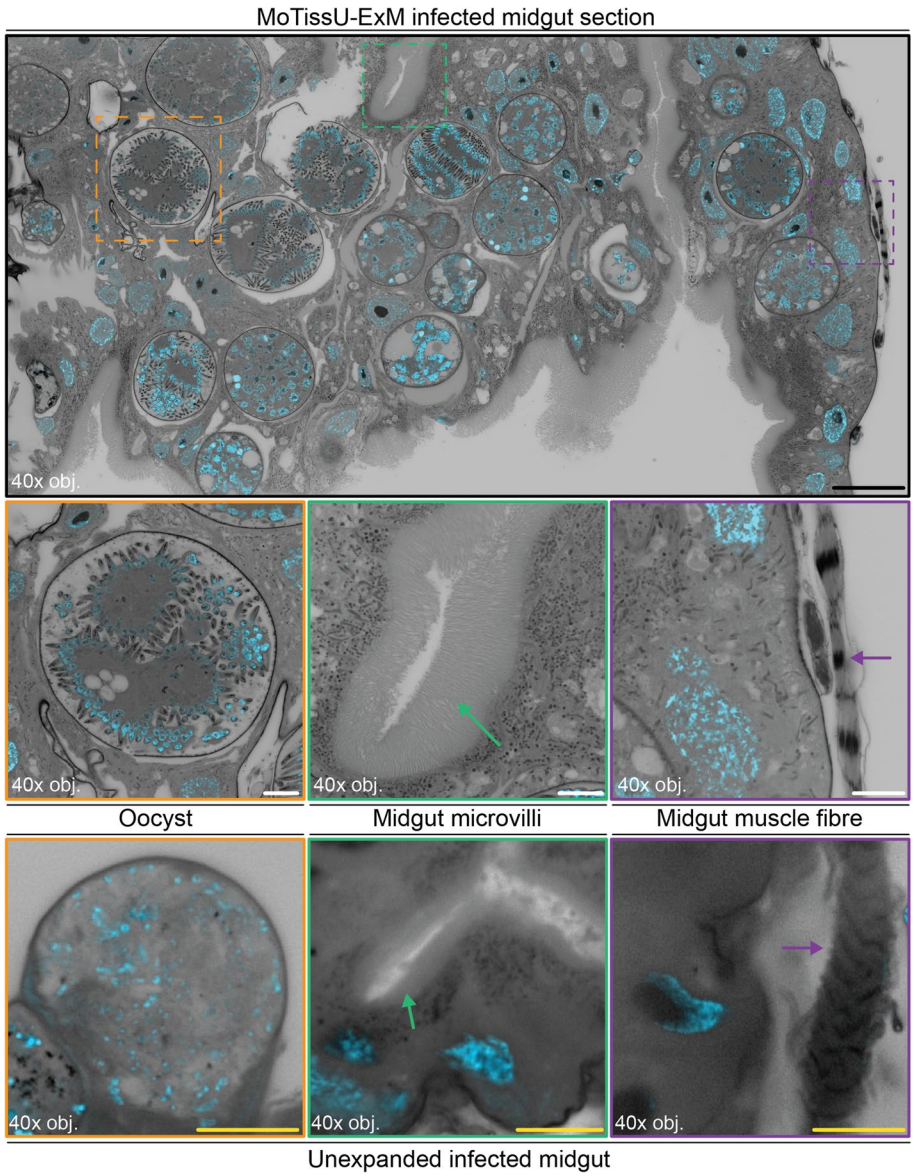

Fig. 5 Mosquito midgut U-ExM preserves both parasite and host ultrastructure. *P. berghei* infected mosquito midguts were prepared by U-ExM, or left unexpanded, stained with SYTOX (cyan, DNA) and NHS ester Alexa Fluor 405 (greyscale, protein density), and imaged by Airyscan Microscopy. From a larger section of the mosquito midgut (black), ultrastructural conservation of both parasite (oocyst, orange) and host (microvilli, green arrows & muscle fibres, magenta arrows) can be observed. Note that images of the unexpanded midgut are not the same midgut prepared by U-ExM. No significant gross, or ultrastructural abnormalities were observed in either the mosquito tissue or parasite following U-ExM. obj. = objective lens. Black scale bar = 100 µm, white scale bar = 20 µm, yellow scale bar = 10 µm. All images are a single z-slice

visualisation of less developed oocysts that have not yet begun sporogony. Additionally, it is possible that MoTissU-ExM could be performed on the midguts of mosquitoes who have recently taken a blood-meal to image ookinetes in situ, but this is outside the scope of this study. Future work will explore imaging of developed ookinetes 24 h post-blood meal, which will likely present unique challenges such as accommodating the enlarged midgut size and addressing the preservation or removal of red blood cells within the blood bolus. This could provide valuable insights into the midgut environment and ookinete development.

Although this protocol was primarily developed for the purpose of imaging malaria parasites along with their mosquito hosts in situ, this protocol holds broader applications for mosquito biology research. It could be used to study mosquito tissues in isolation or to study their interaction with mosquito-borne pathogens, such

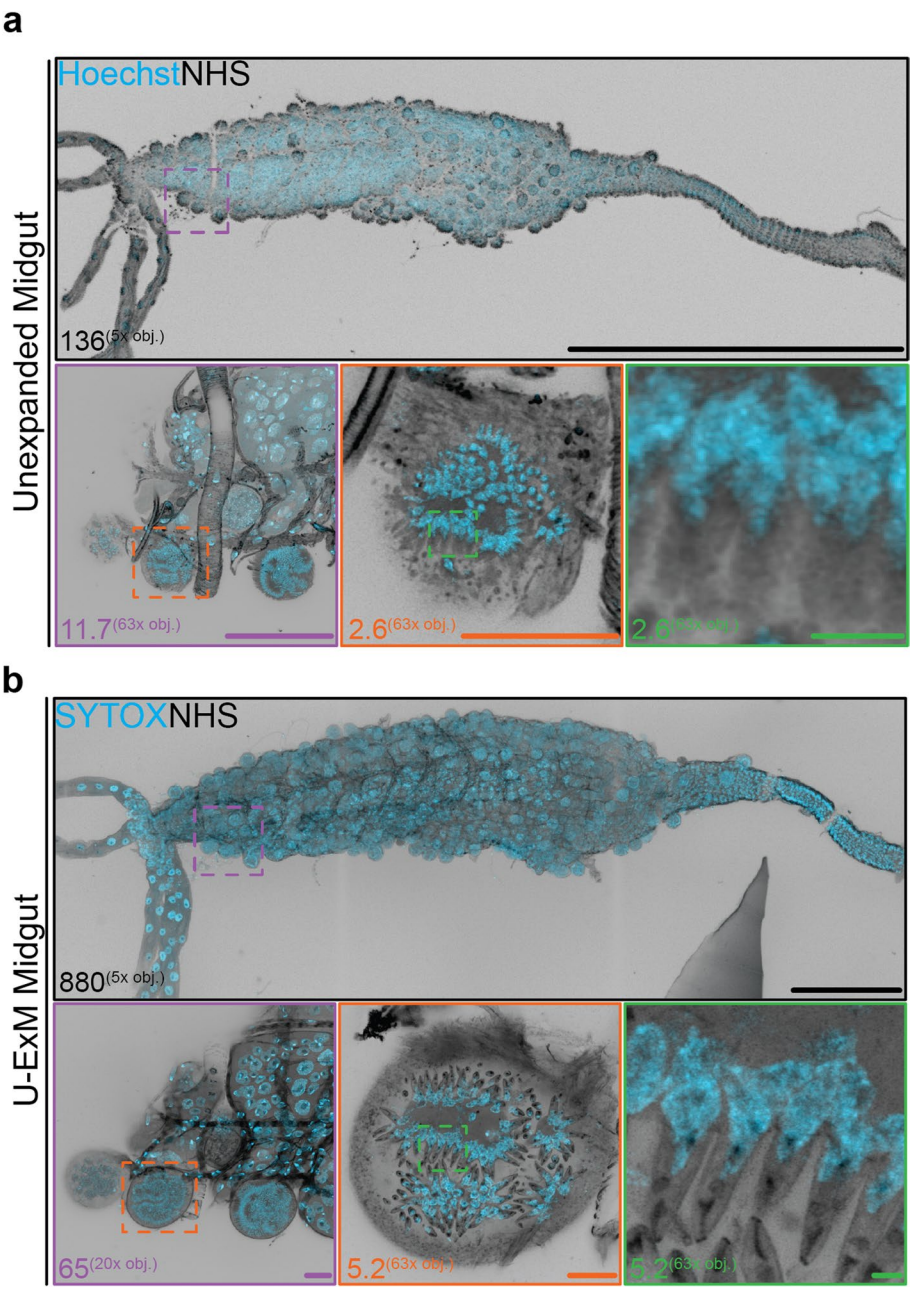

Fig. 6 Imaging of an infected midgut before and after MoTissU-ExM. **a** A mosquito midgut infected with *P. berghei* was fixed, stained with Hoechst (cyan, DNA) and NHS ester Alexa Fluor 405 (greyscale, protein density), and imaged by Airyscan microscopy. The entire midgut (top row), a section of that midgut (magenta), an individual oocyst (orange), and forming sporozoites in that oocyst (green) are all depicted. **b** After imaging, the same midgut, section, and oocyst were prepared by U-ExM, stained with SYTOX (cyan, DNA), re-stained with NHS Ester, and re-imaged. Number in the bottom corner of each image indicates z-projection depth in µm. The projections shown in the zoom panels are only representative of the chosen region of interest and do not display the full depth of the midgut. obj. = objective lens. Scale bars: black = 1000 µm, magenta = 50 µm, orange = 25 µm, green = 5 µm

as *Flaviviridae* and *Aedes* mosquitoes, or filarial worms and *Culex* mosquitoes. More broadly, this protocol could be applied to any vector whose midgut and salivary gland(s) can be easily dissected, including sandflies infected with *Leishmania*, blackflies with *Onchocerca*, tsetse flies and triatomines with trypanosomes, or ticks with any of the various bacteria, viruses, and parasites they transmit.

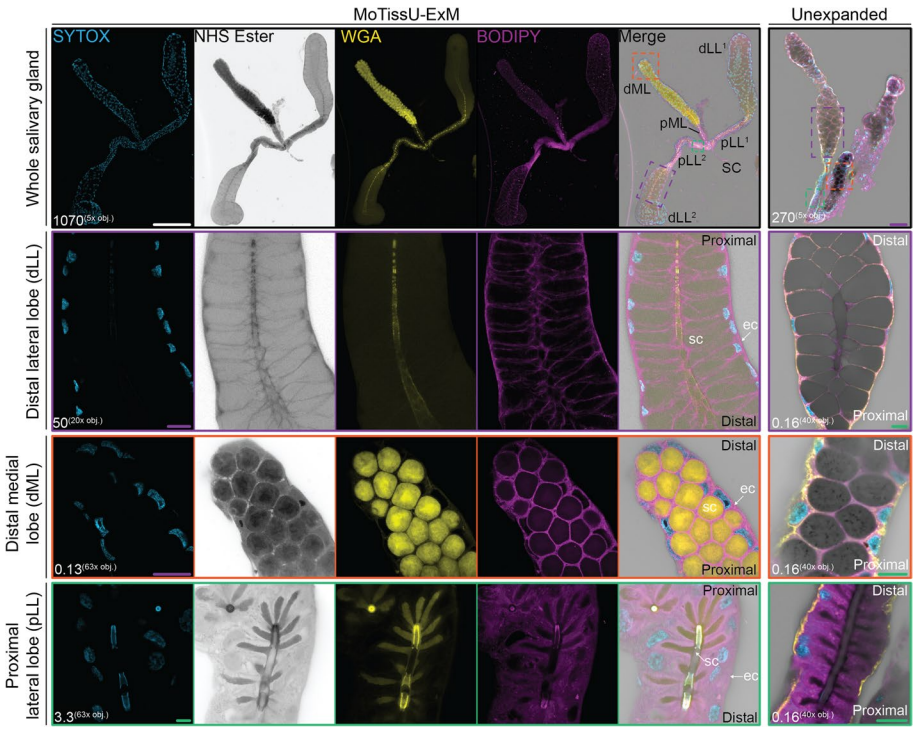

Fig. 7 U-ExM preserves salivary gland anatomical structure and ultrastructure. Mosquito salivary glands were prepared by U-ExM, or left unexpanded, stained with SYTOX (cyan, DNA), NHS ester Alexa Fluor 405 (greyscale, protein density), wheat germ agglutinin Texas red (WGA (yellow, chitin & glycans), and BODIPY FL-Ceramide (magenta, lipids), and imaged by Airyscan Microscopy. In U-ExM salivary glands, all anatomical features were preserved including secretory cavity, and both the distal (d) and proximal (p) regions of the medial lobe (ML) and lateral lobes (LL). Zoomed in regions of a distal lateral lobe (dLL^2, magenta), the distal medial lobe (dML, orange), and a proximal lateral lobe (pLL^2, green) show their ultrastructural preservation and the clear distinction between the epithelial cell cytoplasm (ec) and secretory cavity (sc). Proximal and distal are indicated on zoomed regions to show their orientation. Note that the unexpanded salivary gland is not the same salivary gland prepared by U-ExM. Number in the bottom corner of each image indicates z-projection depth in µm. obj. = objective lens. Scale bars: white = 500 µm, magenta = 50 µm, green = 10 µm

Use of longitudinally opened midguts

We showed that longitudinally opened midguts can be prepared using the MoTissU-ExM protocol. When longitudinally opened, approximately half of prepared midguts would be oriented in a gel in way that dramatically increased the midgut surface area accessible for imaging. The other half, however, would be oriented with the 'opened' side facing towards the cover glass (towards the objective). When in this orientation, almost none of the midgut would be accessible for imaging at high magnification. For example, the unexpanded opened midgut in Fig. 9 required a z-depth more than twice as deep as the closed midgut to capture the entire tissue. However, even considering this limitation there may be some instances where the longitudinal opening of midguts would be favourable for MoTissU-ExM, *i.e.* when burden of parasites per midgut is high, or the number of midguts is not a limiting factor. In this study for example, we exclusively used *P. berghei*, which typically reaches high midgut oocyst burdens well over 100 per midgut [32]. In cases where the oocyst burden is substantially lower, such as for *P. falciparum* [33] or a mutant/drug treated parasite, but the numbers of midguts is not a limiting resource, longitudinally opening midguts may be favourable. By contrast, if the numbers of midguts available for imaging is low, it would not be favourable to longitudinally open these midguts, as approximately 50% of them will not contain imageable oocysts.

Common challenges of imaging MoTissU-ExM samples

The primary challenge in imaging MoTissU-ExM samples lies in the depth of the sample, which poses difficulties for high-resolution imaging. Using a conventional high-resolution objective lens with a high-numerical aperture (1.4 NA), we consistently encountered limitations to image an entire oocyst without exceeding the working distance of the lens. Additionally, we were often unable to access any of the expanded tissue using this imaging setup. Hence, it is advisable to always image samples using long working distance objective lenses. In our opinion, any compromise in resolution due to the use of a lower NA, longer working distance lens, is offset by improved sample

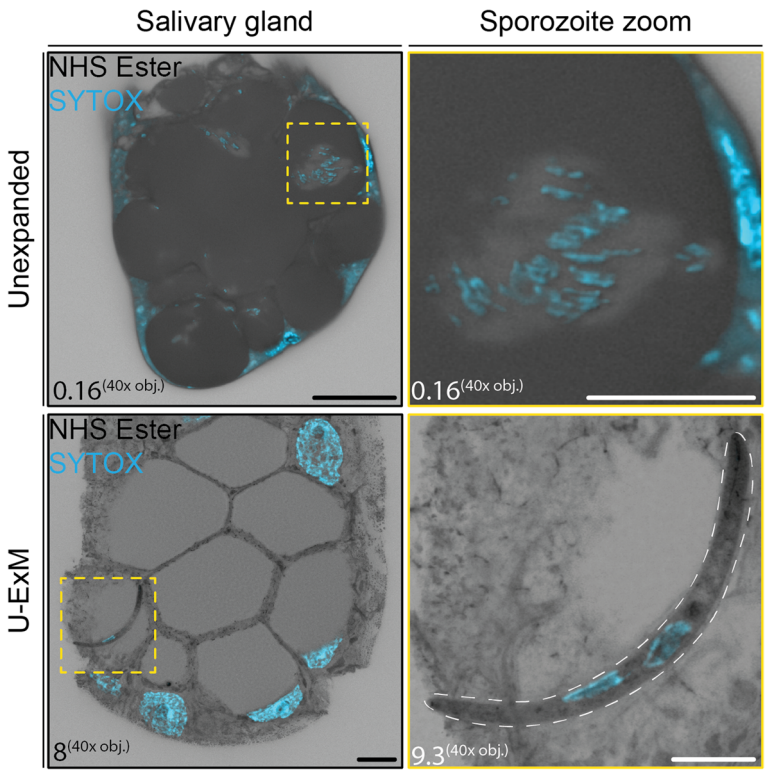

Fig. 8 Comparison of sporozoites in unexpanded and U-ExM salivary glands. Mosquito salivary glands infected with *P. berghei* were fixed, and either imaged unexpanded or prepared by U-ExM. Unexpanded salivary glands were stained with SYTOX (cyan, DNA) and NHS ester Alexa Fluor 405 (greyscale, protein density). U-ExM salivary glands were stained with STYOX and NHS ester. Depicted is a section of the infected salivary gland, along with a zoom of sporozoites inside the salivary gland (yellow). For the U-ExM sporozoite, the parasite plasma membrane is indicated with a white dashed line. Number in the bottom corner of each image indicates z-projection depth in µm. obj. = objective lens. Scale bars: black = 20 µm, white = 10 µm

accessibility. Further, long working distance objectives, such as the 40× objective lens used in this study, are frequently water-immersion objectives. Given that the expanded gel is almost entirely water, using a water-immersion objective lens helps minimise spherical aberration compared to oil-immersion objectives (visible in Fig. 10). Alternatively, MoTissU-ExM samples could be imaged using methods where sample depth is not a significant concern, such as using LightSheet fluorescence microscopy [34].

It has previously been shown that the presence of chitin in tissues can limit expansion, which can be overcome by treating samples with chitinase [22]. In this protocol, we did not treat tissues with chitinase and despite this no significant aberrations in expansion were noticed either at the tissue or cell level. This is likely because the midgut and salivary gland have relatively low amounts of chitin by comparison to the exoskeleton or wing tissue, for example. Within the salivary glands, however, the secretory duct is thought to be highly chitinous [35] and indeed the secretory duct was highly fluorescent using wheat germ agglutinin (WGA), which binds chitin and sialic acid (Fig. 7). To the best of our understanding, chitin should not expand and should not be anchored to the gel using U-ExM so it is unclear why WGA fluorescence is strong in regions thought to be chitinous. One possibility is that in these expanded samples, WGA is not binding chitin and instead the fluorescence of WGA corresponds to sialylated proteins, and that these happen to be similar to the distribution of chitin. It is noteworthy that while the secretory duct is also highly protein dense, the WGA signal is not identical to protein density (Fig. 7), which is a known trait of fluorescent dyes with high background [14]. Currently, the mechanism by which molecules are crosslinked to hydrogels using formaldehyde and acrylamide is not entirely understood [36–38] and so it is unclear whether WGA fluorescence corresponds to chitin, sialylated proteins, or something else.

In the development of MoTissU-ExM, we typically used highly infected midguts and salivary glands to facilitate the detection of parasites within the tissue. When parasite burdens are high, oocysts can easily be found in midguts and sporozoites in salivary glands using either DNA

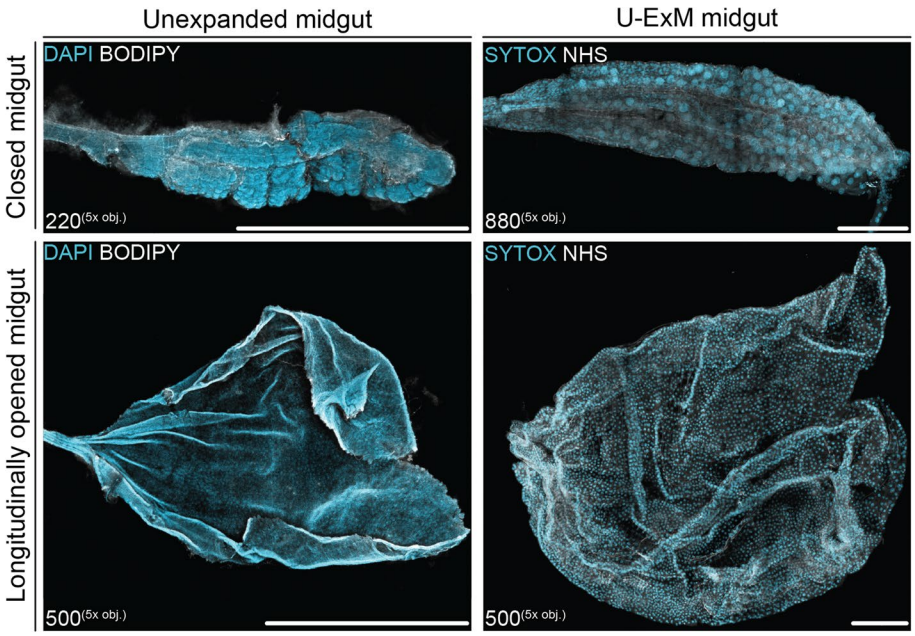

Fig. 9 Longitudinally opened midguts prepared using MoTissU-ExM. During mosquito tissue dissection, midguts were either removed intact (closed) or 'opened' longitudinally. Opened midguts were prepared for U-ExM identically to closed midguts. Unexpanded midguts were stained with DAPI (cyan, DNA) and BODIPY-TR-Ceramide (white, lipids), while U-ExM midguts were stained with SYTOX (cyan, DNA) and NHS Ester Alex Fluor 405 (white, protein density). Number in the bottom corner of each image indicates z-projection depth in µm. obj. = objective lens. Scale bar = 1000 µm

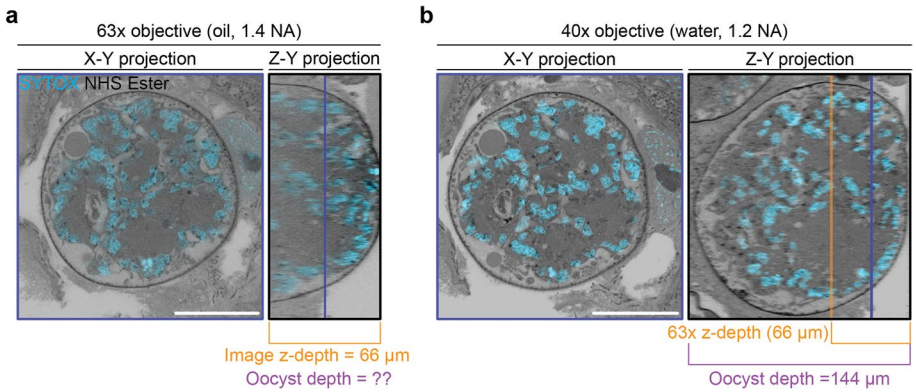

Fig. 10 Comparison of oil and water immersion objectives for imaging expanded samples. A *P. berghei* infected mosquito midgut was prepared by U-ExM, stained with SYTOX (cyan, DNA) and NHS ester Alexa Fluor 405 (greyscale, protein density), and imaged by Airyscan Microscopy. **a** Image of an oocyst using a 63 × oil-immersion objective showing a single X–Y slice and Z-Y projection (3D image rotated 90° to the right). Using this imaging setup, the image z-depth reached 66 µm before exceeding the working distance of the objective. Oocyst depth could not be measured, as it exceeded the image z-depth. **b** The same oocyst imaged using a 40 × water-immersion objective with a longer working distance. Using this imaging setup, the oocyst depth was measured at 144 µm. The blue line indicates the z-axis position of the z-slice depicted in the X–Y projections, while the orange line represents the maximum z-depth imaged using the 63 × objective. Scale bar = 50 µm

or protein density dyes. In cases with low parasite burden, we recommend the use of a parasite-specific marker (such as an anti-capsule antibody or anti-circumsporozoite protein antibody for example), which will allow unambiguous identification of parasites within tissues. In expanded tissues, fluorescent parasites will be visible even at low-magnification so large areas of the tissue can be scanned for parasite-specific fluorescence at low magnification before switching to a high-magnification objective lens for imaging.

Adaptations of U-ExM and iterative U-ExM methods

Our development of MoTissU-ExM mostly focussed on how to dissect mosquito tissues and reliably get them into hydrogels. Considering this, the protocol should be adaptable to the many other forms of expansion microscopy, or experiments multiplexed with expansion microscopy. For example, this protocol could simply be adapted for ten-fold robust expansion microscopy (TREx) [39], MAGNIFY [40], iterativeU-ExM (iUExM) [41], or ExFISH [42]. One caveat to this is that issues of sample depth would be considerably worse for expansion microscopy protocols that result in greater than fourfold one-dimensional expansion. Therefore, if TREx, MAGNIFY, or iUExM were applied to mosquito tissues, for example, it is likely that LightSheet fluorescence microscopy would need to be used to access the sample. One possible alternative to overcoming the issue of sample depth, would be to make transverse sections of a gel and then image the sections. To the best of our knowledge, however, this has not been previously published.

Methods

Mosquito rearing

An. gambiae (Keele strain) [43] mosquitoes were maintained at 27 °C and 80% relative humidity, following a 14-h/10-h light/dark cycle under standard laboratory conditions at the National Institutes of Health.

Mice details and mouse handling

All animal procedures were performed in strict accordance with the National Institutes of Health (NIH) guidelines under protocols approved by the National Institute of Allergy and Infectious Diseases Animal Care and Use Committees (NIAID ACUC). The studies were done following approved animal study proposals LMVR-22. All mice used in this study were Swiss Webster mice purchased from Charles River Laboratories. Mice were sedated by intraperitoneal injection of a saline solution containing 60 mg/kg of ketamine and 5 mg/kg of xylazine. Mice were euthanized with CO_2 in accordance with ARAC Guidelines and CMB SOP 6601.

Parasite strains

All experiments in this study were performed using a *Plasmodium berghei* ANKA strain genetically modified to express a green fluorescent protein (GFP) driven by the elongation factor 1A (ef1α) promoter [44, 45]) in the background of either *ron11*^{cKD} or *ron11*^{ctrl} parasites.

Mosquito infections

For infection female mosquitoes, aged 4–5 days, were allowed to feed on *P. berghei*-infected mice with an exflagellation rate of 3–4 exflagellants per 40× microscopic field. After three to four days at 19°C, the mosquitoes were allowed to lay eggs.

Sample preparation & fixation

Midguts

Mosquito midguts were dissected in in phosphate-buffered saline (PBS, 130 mM NaCl, 7 mM Na_2HPO_4, 3 mM NaH_2PO_4·H2O pH 7.2) at room temperature. Midguts were subsequently immersed in 4% paraformaldehyde in PBS after dissection.

Longitudinally opened midguts

For longitudinally opened midguts, mosquitoes were allowed to feed on freshly prepared 10% BSA in 0.15 M Sodium Chloride mixed with 10 mM sodium bicarbonate, pH 7.2 [46, 47]. Midguts were subsequently fixed for 30 s in 4% paraformaldehyde (PFA). Midguts were then opened longitudinally using a pair of number 5 dissecting forceps. After opening, midguts were fixed for 1 h with 4% PFA in PBS.

Salivary glands

Salivary glands were dissected PBS at room temperature before being immediately fixed with 4% PFA in PBS.

Mosquito tissue ultrastructure expansion microscopy (MoTissU-ExM)

A full, step-by-step protocol for performing MoTissU-ExM, including imaging tips, troubleshooting, and FAQ, can be found in the Supplementary Information.

Briefly, fixed dissected midguts or salivary glands were placed in anchoring solution (1.2% acrylamide, 2% formaldehyde in PBS) and incubated overnight at 37 °C. After anchoring, dissected tissues were place on 12 mm round Poly-D-Lysine coated coverslips. Coverslips containing anchored tissues, were transferred into a gel made of activated monomer solution (19% wt/wt sodium acrylate, 10% acrylamide, 0.1% Bisacrylamide, 0.5% TEMED, 0.5% ammonium persulphate, in PBS). Gels were polymerised at 37 °C for 30 min before being transferred to a 6-well plate containing denaturation buffer (200 mM SDS, 200 mM NaCl, 50 mM Tris, pH9, in water) with agitation for 15 min. Once gels had separated from their coverslip, individual tissues were cut out of the gel and placed into a 1.5 mL tube containing denaturation buffer and heated at 95 °C for 90 min. Denatured tissues were then fully expanded in 3×30 min washes in deionised water. Expanded gels were shrunk down by washing 2×15 min in PBS for antibody/dye staining. Primary antibodies were incubated overnight at room temperature, while secondary antibodies and other dyes were incubated for 2.5 h at room temperature in the dark. After either antibody staining, gels were washed 3×10

min in 0.5% PBS-Tween-20. After antibody staining, gels were re-expanded by 3×30 min washes in deionised water. For gels stained with BODIPY-TR or FL ceramide, fully expanded gels were incubated in BODIPY-TR/FL ceramide overnight in 0.2% propyl gallate in water. Stained gels were transferred to Poly-D-lysine coated dishes for imaging.

Image acquisition

All images in this study were acquired using an LSM900 AxioObserver with Airyscan 2 (Zeiss, Oberkochen, Germany). Images were acquired on either a 5×Fluar (air, 0.25 NA), 20×Plan-apochromat (air, 0.8 NA), 40×C-apochromat autocorr M27 (water, 1.2 NA), or 63×Plan-apochromat (oil, 1.4 NA). The objective used for each image in this study is indicated in the bottom left corner of the image.

Image processing and presentation

All images in this study underwent Airyscan processing using 'moderate' filter strength. Images acquired using the 5×and 20×objectives underwent 2D Airyscan processing, while images acquired using either the 40×or 63×objectives underwent 3D Airyscan processing. For images that contain NHS Ester, the gamma value of this channel was set to 0.45, rather than 1 for greater discernment of subcellular structures; as has previously been described [14].

All images in this study were prepared and processed in, then exported from ZEN Blue Version 3.5 (Zeiss, Oberkochen, Germany). Images in Figs. 2a, 3a, 5b, 6, 7, & 10 were rotated and/or cropped from a larger original image to aid comparison.

Unexpanded tissue imaging

Unexpanded midguts or salivary glands were dissected and fixed as described in the point-by-point protocol. Fixed tissues were then washed in PBS to remove the fixative and stained with Hoechst, SYTOX, NHS Ester Alexa Fluor 405, or BODIPY-FL-Ceramide diluted in PBS for 1 h at room temperature. Stained tissues were then transferred to Poly-D-Lysine coated 35 mm imaging dishes with 22 mm #1.5 cover glass bottoms, covered with ProLong Glass and imaged using Airyscan Microscopy.

Imaging of tissues before and after U-ExM

For the salivary glands and midguts that were imaged both before and after U-ExM, the tissues were initially prepared as described for unexpanded tissue imaging except without Poly-D-lysine coating the imaging dishes. These tissues were then imaged immediately after application of ProLong Glass. Once imaging was complete, imaging dishes were washed multiple times with PBS until the tissues detached from the imaging dish. Detached tissues were further washed in PBS overnight. Once washed, tissues were transferred to anchoring solution and prepared for U-ExM as described in the point-by-point protocol. During imaging, these tissues were intentionally oriented in a manner similar to the unexpanded image to aid comparison.

Measurement of nucleus diameter

To measure nucleus diameter, the slice at which each nucleus had its maximum diameter was found and this diameter was measured manually in 2D using the 'Profile' function of ZEN Blue. Only one diameter measurement was made per nucleus. Measurement histograms were imprinted on top of measured nuclei to prevent repeated measurements of the same nucleus.

Isolated sporozoite U-ExM

P. berghei sporozoites were isolated from salivary glands as previously described [33] before being fixed in 4% paraformaldehyde and settled on Poly-D-lysine coated 12 mm-round coverslips. Once sporozoites had settled onto coverslips, they were prepared for U-ExM as previously described [4, 6, 14] and imaged as described above.

Statistical analysis

All graphs presented in this study were generated using GraphPad PRISM (version 10). All error bars represent standard deviation. On both graphs, large datapoints represent mean values of nucleus diameter from a single

Table 1 Summary of all antibodies used in this study

Antibody (Ab)	Ab species	Ab source	Ab concentration	Step of protocol applied	Reference/cat no
Anti-*Pb*circumsporozoite protein (3D11)	Mouse	BEI Resources	1: 1000	Primary Ab	MRA-100A [48]
Anti-mouse IgG Alexa Fluor 555 (H + L)	Goat	Invitrogen	1:500 (2mg/ml stock)	Second Ab	A21422
Anti-mouse IgG Alexa Fluor 488 Superclonal (H + L)	Goat	Invitrogen	1:500 (1mg/ml)	Second Ab	A28175

Table 2 Summary of all fluorescent dyes and stains used in this study. *Indicates that dye was also used on unexpanded samples

Stain/dye	Source	Concentration	Step of protocol applied	Cat no
NHS Ester Alexa Fluor 405	ThermoFisher	1:250 (2 mg/mL stock in DMSO)	Secondary Ab*	A30000
BODIPY-TR-Ceramide	ThermoFisher	1:500 (1 mM stock in DMSO)	Post expansion	D7540
BODIPY-FL-C_5-Ceramide	ThermoFisher	1:500 (1 mM stock in DMSO)	Post expansion*	D3521
SYTOX Deep Red	ThermoFisher	1:1000 (1 mM stock in DMSO)	Secondary Ab*	S11381
Wheat Germ Agglutinin Texas Red-X	ThermoFisher	1:250 (1 mg/mL stock in PBS)	Post expansion	W21405
Hoechst 33,342	ThermoFisher	1:1000 (10 mg/mL stock in water)	Unexpanded only	C10329G

tissue, while small datapoints represent diameter measurements of individual nuclei.

1D-expansion factor was estimated by dividing the mean expanded nucleus diameter (31.62 µm for midguts, 42.63 µm for salivary glands) by the mean unexpanded nucleus diameter (7.25 µm for midguts, 10.17 µm for salivary glands).

Stains and antibodies

A list of stains and antibodies used in this study, along with their working concentrations, source and step of application is listed in Tables 1 and 2.

Supplementary Information

The online version contains supplementary material available at https://doi.org/10.1186/s44330-024-00013-4.

Supplementary Material 1.

Acknowledgements

We thank Prof. Tomoko Ishino (Tokyo Medical & Dental University) for generously providing the *P. berghei* RON11^{ctrl} parasites that were used for some of the infections in this study. This work is supported by an AHA Postdoctoral Fellowship (23POST1011626, BL). We thank the IUSM Pharmacology & Toxicology department for facilitating travel between labs through the Career Development Award. We thank Matt Curtis (PhD) and Michael Hester (PhD) (Zeiss Microscopy, White Plains, NY, USA) for their demonstration of a 40× water-immersion objective, helpful discussions about imaging and their expertise in microscopy optics. We thank Dr. Claire Sayers (University of New South Wales) and Annika Binder (Heidelberg University) for their thoughtful feedback on the manuscript. Anti-CSP antibodies were obtained through BEI Resources, NIAID, NIH.

Authors' contributions

Author Contributions using the CREDiT taxonomy system are as follows: Benjamin Liffner – Conceptualisation, Data curation, Formal analysis, Funding acquisition, Investigation, Methodology, Visualisation, Writing – original draft, Writing – review & editing. Thiago Luiz Alves e Silva – Conceptualisation, Formal Analysis, Investigation, Methodology, Writing – original draft, Writing – review & editing. Joel Vega-Rodriguez – Conceptualisation, Funding acquisition, Resources, Supervision, Writing – review & editing. Sabrina Absalon – Conceptualisation, Funding acquisition, Resources, Supervision, Writing – review & editing.

Funding

BL was funded by an American Heart Association Postdoctoral Fellowship (23POST1011626). Travel of BL to travel to the lab of JV-R was supported by the Indiana University School of Medicine, Department of Pharmacology & Toxicology Career Development Grant.

Availability of data and materials

The images that were taken for the development of the technique described in this manuscript form a small part of a much larger imaging dataset of an as yet unpublished study. Upon publication, all images will be placed onto a publicly available database. Until this time, the authors agree to share all images that were not included in the figures of the manuscript upon request.

Declarations

Ethics approval and consent to participate

All animal procedures were performed in strict accordance with the National Institutes of Health (NIH) guidelines under protocols approved by the National Institute of Allergy and Infectious Diseases Animal Care and Use Committees (NIAID ACUC). The studies were done following approved animal study proposals LMVR-22. Mice were euthanized with CO_2 in accordance with ARAC Guidelines and CMB SOP 6601.

Consent for publication

Not applicable.

Competing interests

The authors declare no competing interests

Received: 18 April 2024 Accepted: 26 September 2024
Published online: 07 October 2024

References

1. Huang B, Babcock H, Zhuang X. Breaking the diffraction barrier: super-resolution imaging of cells. Cell. 2010;143:1047–58. https://doi.org/10.1016/j.cell.2010.12.002.
2. Sydor AM, Czymmek KJ, Puchner EM, Mennella V. Super-resolution microscopy: from single molecules to supramolecular assemblies. Trends Cell Biol. 2015;25:730–48. https://doi.org/10.1016/j.tcb.2015.10.004.
3. Chen F, Tillberg PW, Boyden ES. Expansion microscopy. Science. 2015;347:543–8. https://doi.org/10.1126/science.1260088.
4. Gambarotto D, et al. Imaging cellular ultrastructures using expansion microscopy (U-ExM). Nat Methods. 2019;16:71–4. https://doi.org/10.1038/s41592-018-0238-1.
5. Hinterndorfer K, et al. Ultrastructure expansion microscopy reveals the cellular architecture of budding and fission yeast. J Cell Science. 2022;135:jcs260240. https://doi.org/10.1242/jcs.260240.

6. Bertiaux E, et al. Expansion microscopy provides new insights into the cytoskeleton of malaria parasites including the conservation of a conoid. PLoS Biol. 2021;19:e3001020. https://doi.org/10.1371/journal.pbio.3001020.
7. Guérin A, et al. Cryptosporidium uses multiple distinct secretory organelles to interact with and modify its host cell. Cell Host and Microbe. 2023;31:650-664.e656. https://doi.org/10.1016/j.chom.2023.03.001.
8. Tosetti N, et al. Essential function of the alveolin network in the subpellicular microtubules and conoid assembly in *Toxoplasma gondii*. eLife. 2020;9:e56635. https://doi.org/10.7554/eLife.56635.
9. Klena, N. et al. An In-depth Guide to the Ultrastructural Expansion Microscopy (U-ExM) of Chlamydomonas reinhardtii. Bio Protoc 13, e4792 (2023). https://doi.org/10.21769/BioProtoc.4792
10. Olivetta M, Bhickta C, Chiaruttini N, Burns J, Dudin O. A multicellular developmental program in a close animal relative. bioRxiv, 2024.2003.2025.586530 (2024). https://doi.org/10.1101/2024.03.25.586530
11. Shah H, et al. Life cycle-coupled evolution of mitosis in close relatives of animals. bioRxiv. 2023.2005.2010.540163 (2023). https://doi.org/10.1101/2023.05.10.540163.
12. Reza MH, et al. Expansion microscopy reveals unique ultrastructural features of pathogenic budding yeast species. bioRxiv. 2024.2002.2020.581313 (2024). https://doi.org/10.1101/2024.02.20.581313
13. Liffner B, Absalon S. Expansion microscopy of apicomplexan parasites. Mol Microbiol. https://doi.org/10.1111/mmi.15135.
14. Liffner B, et al. Atlas of *Plasmodium falciparum* intraerythrocytic development using expansion microscopy. eLife. 2023. https://doi.org/10.7554/elife.88088.1.
15. Cepeda_Diaz AK, Rudlaff RM, Farringer M, Dvorin JD. Essential function of alveolin *Pf*IMC1g in the *Plasmodium falciparum* asexual blood stage. mBio 0, e01507–01523 https://doi.org/10.1128/mbio.01507-23
16. Dos Santos Pacheco N, et al. Sustained rhoptry docking and discharge requires *Toxoplasma gondii* intraconoidal microtubule-associated proteins. Nat Commun. 2024;15:379. https://doi.org/10.1038/s41467-023-44631-y.
17. Oliveira Souza RO, Jacobs KN, Back PS, Bradley PJ, Arrizabalaga G. IMC10 and LMF1 mediate mitochondrial morphology through mitochondrion-pellicle contact sites in Toxoplasma gondii. J Cell Sci. 2022;135:jcs260083. https://doi.org/10.1242/jcs.260083.
18. John, A. *et al.* Conservation, abundance, glycosylation profile, and localization of the TSP protein family in *Cryptosporidium parvum*. J Biol Chemistry 299 (2023). https://doi.org/10.1016/j.jbc.2023.103006
19. Tomasina R, González FC, Echeverría S, Cabrera A, Robello C. Insights into the cell division of Neospora caninum. Microorganisms. 2023;12:61. https://doi.org/10.3390/microorganisms12010061.
20. Steib E, et al. TissUExM enables quantitative ultrastructural analysis in whole vertebrate embryos by expansion microscopy. Cell Reports Methods. 2022;2:100311. https://doi.org/10.1016/j.crmeth.2022.100311.
21. Liffner B, Absalon S. Expansion microscopy reveals *Plasmodium falciparum* blood-stage parasites undergo anaphase with a chromatin bridge in the absence of mini-chromosome maintenance complex binding protein. Microorganisms. 2021;9:2306.
22. Jiang N, et al. Superresolution imaging of *Drosophila* tissues using expansion microscopy. Mol Biol Cell. 2018;29:1413–21. https://doi.org/10.1091/mbc.E17-10-0583.
23. Simon CS, et al. An extended DNA-free intranuclear compartment organizes centrosome microtubules in malaria parasites. Life Sci Alliance. 2021;4:e202101199. https://doi.org/10.26508/lsa.202101199.
24. Li J, et al. Disruption of Plasmodium falciparum kinetochore proteins destabilises the nexus between the centrosome equivalent and the mitotic apparatus. Nat Commun. 2024;15(1):5794.
25. Kudryashev M, et al. Positioning of large organelles by a membrane- associated cytoskeleton in Plasmodium sporozoites. Cell Microbiol. 2010;12:362–71. https://doi.org/10.1111/j.1462-5822.2009.01399.x.
26. Schrevel J, et al. Vesicle trafficking during sporozoite development in *Plasmodium berghei*: ultrastructural evidence for a novel trafficking mechanism. Parasitology. 2008;135:1–12. https://doi.org/10.1017/s0031182007003629.
27. Singer M, Frischknecht F. Fluorescent tagging of Plasmodium circumsporozoite protein allows imaging of sporozoite formation but blocks egress from oocysts. Cell Microbiol. 2021;23.
28. Cyrklaff M, et al. Cryoelectron tomography reveals periodic material at the inner side of subpellicular microtubules in apicomplexan parasites. J Exp Med. 2007;204:1281–7. https://doi.org/10.1084/jem.20062405.
29. Araki T, et al. Three-dimensional electron microscopy analysis reveals endopolygeny-like nuclear architecture segregation in Plasmodium oocyst development. Parasitol Int. 2020;76:102034. https://doi.org/10.1016/j.parint.2019.102034.
30. Baia-da-Silva DC, et al. Microanatomy of the American malaria vector *Anopheles aquasalis* (Diptera: Culicidae: Anophelinae) midgut: ultrastructural and histochemical observations. J Med Entomol. 2019;56:1636–49. https://doi.org/10.1093/jme/tjz114.
31. Orfano AS, et al. Species-specific escape of *Plasmodium* sporozoites from oocysts of avian, rodent, and human malarial parasites. Malar J. 2016;15:394. https://doi.org/10.1186/s12936-016-1451-y.
32. Klug D, Frischknecht F. Motility precedes egress of malaria parasites from oocysts. Elife. 2017;6:e19157. https://doi.org/10.7554/eLife.19157.
33. Alves e Silv TL, et al. The fibrinolytic system enables the onset of *Plasmodium* infection in the mosquito vector and the mammalian host. Sci Adv. 2021;7(6):eabe3362. https://doi.org/10.1126/sciadv.abe3362.
34. Stelzer EHK, et al. Light sheet fluorescence microscopy. Nat Rev Methods Primers. 2021;1:73. https://doi.org/10.1038/s43586-021-00069-4.
35. Wells MB, Villamor J, Andrew DJ. Salivary gland maturation and duct formation in the African malaria mosquito *Anopheles gambiae*. Sci Rep. 2017;7:601. https://doi.org/10.1038/s41598-017-00672-0.
36. Chung K, et al. Structural and molecular interrogation of intact biological systems. Nature. 2013;497:332–7. https://doi.org/10.1038/nature12107.
37. Ku T, et al. Multiplexed and scalable super-resolution imaging of three-dimensional protein localization in size-adjustable tissues. Nat Biotechnol. 2016;34:973–81. https://doi.org/10.1038/nbt.3641.
38. Wen G, Leen V, Rohand T, Sauer M, Hofkens J. Current progress in expansion microscopy: chemical strategies and applications. Chem Rev. 2023;123:3299–323. https://doi.org/10.1021/acs.chemrev.2c00711.
39. Damstra HGJ, et al. Visualizing cellular and tissue ultrastructure using Ten-fold Robust Expansion Microscopy (TREx). Elife. 2022;11. https://doi.org/10.7554/eLife.73775
40. Klimas A, et al. Magnify is a universal molecular anchoring strategy for expansion microscopy. Nat Biotechnol. 2023;41:858–69. https://doi.org/10.1038/s41587-022-01546-1.
41. Louvel V, et al. iU-ExM: nanoscopy of organelles and tissues with iterative ultrastructure expansion microscopy. Nat Commun. 2023;14:7893. https://doi.org/10.1038/s41467-023-43582-8.
42. Chen F, et al. Nanoscale imaging of RNA with expansion microscopy. Nat Methods. 2016;13:679–84. https://doi.org/10.1038/nmeth.3899.
43. Hurd H, Taylor PJ, Adams D, Underhill A, Eggleston P. Evaluating the costs of mosquito resistance to malaria parasites. Evolution. 2005;59:2560–72.
44. Franke-Fayard B, et al. A *Plasmodium berghei* reference line that constitutively expresses GFP at a high level throughout the complete life cycle. Mol Biochem Parasitol. 2004;137:23–33. https://doi.org/10.1016/j.molbiopara.2004.04.007.
45. Bantuchai S, et al. Rhoptry neck protein 11 has crucial roles during malaria parasite sporozoite invasion of salivary glands and hepatocytes. Int J Parasitol. 2019;49:725–35. https://doi.org/10.1016/j.ijpara.2019.05.001.
46. Barletta ABF, Trisnadi N, Ramirez JL, Barillas-Mury C. Mosquito midgut prostaglandin release establishes systemic immune priming. iScience. 2019;19:54–62. https://doi.org/10.1016/j.isci.2019.07.012.
47. Han YS, Thompson J, Kafatos FC, Barillas-Mury C. Molecular interactions between *Anopheles stephensi* midgut cells and *Plasmodium berghei*: the time bomb theory of ookinete invasion of mosquitoes. Embo j. 2000;19:6030–40. https://doi.org/10.1093/emboj/19.22.6030.
48. Cochrane AH, Aikawa M, Jeng M, Nussenzweig RS. Antibody-induced ultrastructural changes of malarial sporozoites. J Immunol. 1976;116:859–67.

Publisher's Note